

Structural, dielectric and multiferroic properties of Er and La substituted BiFeO₃ ceramics

PRAGYA PANDIT, S SATAPATHY*, POORVA SHARMA, P K GUPTA,
S M YUSUF[†] and V G SATHE^{††}

Laser Materials Development & Devices Division, Raja Ramanna Centre for Advanced Technology, Indore 452 013, India

[†]Solid State Physics Division, Bhabha Atomic Research Centre, Mumbai 400 085, India

^{††}UGC-DAE Consortium for Scientific Research, Indore 452 017, India

MS received 6 April 2010; revised 28 May 2010

Abstract. Erbium (Er) and lanthanum (La) substituted BiFeO₃ (BFO) ceramics have been prepared through conventional solid solution route. X-ray diffraction data indicated a gradual phase transition from rhombohedral to monoclinic structure in Bi_{0.9-x}La_{0.1}Er_xFeO₃ ($x = 0.05, 0.07$ and 0.1) (BLEFO_{x = 0.05, 0.07, 0.1}) ceramics. Differential thermal analysis (DTA) measurements of BFO samples showed a ferroelectric transition at 835°C, whereas it is shifted to 792°C for BLEFO_{x = 0.1}. The Raman spectra of BLEFO_{x = 0.05, 0.07, 0.1} samples showed the shift of Raman modes to higher wavenumbers and suppression of A₁ modes indicating decrease in ferroelectricity. The Raman spectra also indicated the structural transformation due to Er and La substitution in BFO. On subsequent erbium doping, the intrinsic dielectric constant is found to decrease from 68 (for pure BFO) to 52 for BLEFO_{x = 0.05} to 43 for BLEFO_{x = 0.07} but increased to 89 for BLEFO_{x = 0.1} when compared to pure BFO. The increase in Er content resulted in the increase in spontaneous magnetization (0.1178 emu/g at 8T for BLEFO_{x = 0.1}) due to collapse of spin cycloid structure. Ferroelectric remnant polarization of BLEFO_{x = 0.05} and BLEFO_{x = 0.07} decreases when compared to pure BFO while small remnant polarization (close to paraelectric behaviour) is evident for BLEFO_{x = 0.1}.

Keywords. BiFeO₃; multiferroics; magnetism; ferroelectricity.

1. Introduction

Recently there is intrigued interest in the emerging novel group of materials called multiferroics because of their promising application in fundamental research and various possible technological schemes (Cheong and Mostovoy 2007; Eerenstein *et al* 2006). Due to the simultaneous coexistence of ferroelectric, ferromagnetic and ferroelastic phases these materials exhibit collective responses to the electric, magnetic and stress fields. However, there are serious material-related problems that obstruct the use of these materials for practical applications. The most common means of achieving ferromagnetism is rarely compatible with ferroelectricity because the requirement of localized transition metal *d* electrons for magnetism is not compatible with second-order Jahn Teller effects which requires empty *d* orbitals for ferroelectricity (Hill 2004). Further, most of the magnetic ferroelectrics tend to have low temperature of magnetic phase transition and are antiferromagnetic. Among the multiferroics, bismuth ferrite (BFO) is the most promising candidate showing

multiferroic properties at room temperature, T_c at 1100, (Ederer and Spaldin 2005; Neaton *et al* 2005) and T_N at ~640 (Fischer *et al* 1980; Sosnowska *et al* 1992). The variable oxidation states of Fe ions (Fe²⁺ to Fe³⁺) which create oxygen vacancies for charge compensation is the source of relatively high conductivity in BFO. However, the resistivity of BFO depends on preparation conditions. Thin films, single crystals and quenched ceramics of BFO having high resistivity suitable for carrying out ferroelectric measurements have also been reported (Eerenstein *et al* 2005; Zhang *et al* 2005; Lee *et al* 2008; Lebeugle *et al* 2008). Similarly the magnetic order is essentially *G* type canted antiferromagnetism but in addition the direction of the magnetic moment rotates with a long wavelength of 620 Å which results in zero remnant magnetization. However, there are reports of coexistence of ferroelectricity and magnetism in BFO which is induced by the rare earth substitution in the A and B site of the perovskite structure. Rare earth ions such as La³⁺, Sm³⁺ and Nd³⁺ (Yuan *et al* 2006; Zhang *et al* 2006; Yuan *et al* 2007) have been added at the A-site and Nb⁵⁺, Mn⁴⁺, Ti⁴⁺ or Cr³⁺ (Jun *et al* 2005; Chung *et al* 2006; Qi *et al* 2005; Singh *et al* 2006; Zhang *et al* 2010) at the B-site for enhancing the electrical and magnetic properties of BFO.

*Author for correspondence (srinu73@rrcat.gov.in)

Rare earth substituted BFO are of enormous importance as magnetoelectric materials due to their significant role in tailoring the electrical and magnetic properties of BFO.

Rare earth element Er is an amphoteric dopant. It acts as an acceptor or donor depending on the A or B site substitution. In BaTiO_3 there is possibility of substitution of both Ba and Ti by Er. Some questions arise: whether Er substitutes Bi or Fe when it is doped in BFO? Does spin cycloid structure get affected by Er doping? Such queries motivated us to study the effect of Er doping on structural, dielectric and magnetic properties of BFO. So far many of the rare earth ions have been doped at the A-site and the B-site, but there is no report on substitution of bismuth (Bi) by erbium (Er).

In this communication we report a study of Er and La doped BFO ceramics. The ionic radius of La is greater than Bi by 0.014 nm and the ionic radius of Er is smaller than that of Bi by 0.014 nm approximately. So it is expected that the volume of the unit cell of BFO should remain same approximately with simultaneous doping of Er and La. $\text{Bi}_{0.9-x}\text{La}_{0.1}\text{Er}_x\text{FeO}_3$ ($x = 0.05, 0.07, 0.1$) ($\text{BLEFO}_{x=0.05,0.07,0.1}$) ceramic pellets were prepared through solid state reaction. The structural transitions of doped BFO samples have been described in this report. The site occupancy of Er has also been investigated by increasing the doping percentage of Er at fixed doping percentage of La. The dielectric and ferroelectric behaviour of BFO and $\text{BLEFO}_{x=0.05,0.07,0.1}$ have also been reported. Enhanced magnetic properties due to doping of La and Er in BFO have also been reported.

2. Experimental

Polycrystalline pure and rare earth doped BFO samples were prepared using a conventional two-step sintering process. The dried oxide reagents Bi_2O_3 (99.99%), Fe_2O_3 (99.99%), Er_2O_3 (99.999%), La_2O_3 (99.99%) were wet mixed together and ball milled for 12 h using isopropyl alcohol as solvent. The powder was doubly calcined consecutively at 650°C for 1 h and 810°C for 1.5 h with intermediate grinding in between to achieve the desired phase. The calcined powders were leached with dilute HNO_3 (Kumar *et al* 2000) followed by multiple washing with deionized water. The leached powders were mechanically pressed at 300 MPa to form 4 mm thick and 15 mm diameter pellets. Rapid sintering was performed in Bi_2O_3 atmosphere in order to minimize losses due to bismuth evaporation. Sintering conditions were optimized and sintering was carried out at 850°C to obtain high density and better dielectric properties.

X-ray diffraction was carried out to identify the crystal structure and to detect any impurity phase in the sample using X-ray diffractometer (Rigaku). Simulation of crystal structure for lattice parameter calculation and crystal structure identification based on the measured X-ray dif-

fraction data was carried out using refinement software (MS modeling). Calorimetric measurements were carried out using DTA (SETARAM model No TG/DTA-92B) to identify T_N and T_c in the given compositions. Dielectric studies were performed as a function of frequency (100 Hz–10⁶ Hz) on Novocontrol alpha-ANB impedance analyzer. The Raman measurements on $\text{BLEFO}_{x=0.05,0.07,0.1}$ samples were carried out using 488 nm excitation source by (LABRAM-HR) spectrometer equipped with a Peltier cooled charge coupled device (CCD detector). The typical spectral resolution was $\sim 1 \text{ cm}^{-1}$. Magnetization measurements were carried out using a 12-T commercial (Oxford 5 instruments) vibrating-sample magnetometer (VSM) as a function of magnetic field. Ferroelectric measurements were carried out using a ferroelectric loop tracer based on Sawyer–Tower circuit.

3. Results and discussions

3.1 Structural analysis

Figure 1 shows the X-ray diffraction patterns of pure BFO and $\text{BLEFO}_{x=0.05,0.07,0.1}$. The experimental XRD

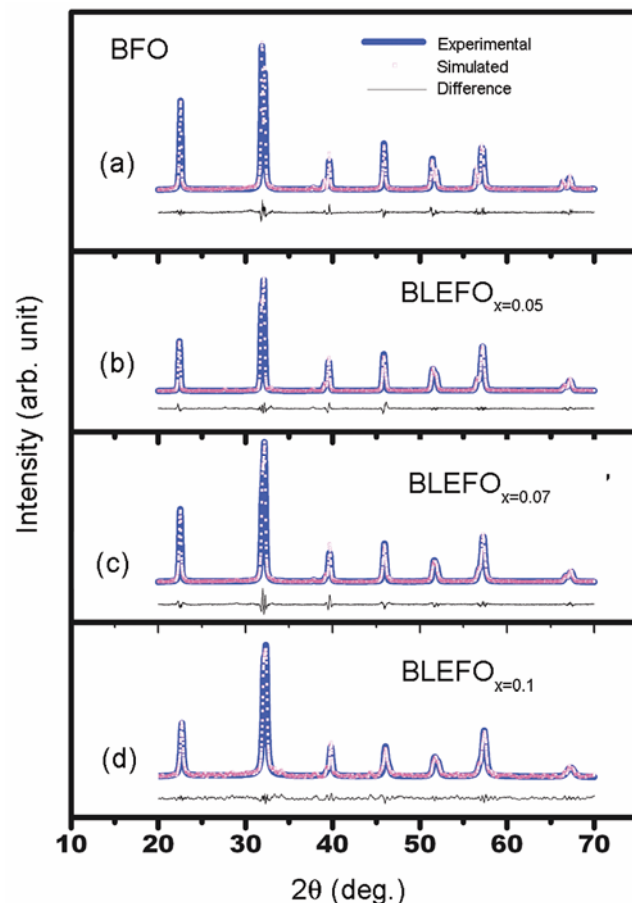


Figure 1. The measured and simulated XRD patterns of (a) BFO; (b) $\text{BLEFO}_{x=0.05}$; (c) $\text{BLEFO}_{x=0.07}$; and (d) $\text{BLEFO}_{x=0.1}$.

Table 1. Crystal structure parameters of BFO and $\text{BLEFO}_{x=0.05,0.07,0.1}$ ceramics obtained from refinement of experimental XRD data.

Compound	Structure	a (Å)	b (Å)	c (Å)	α^0	β^0	γ^0	Volume (Å) 3
BFO	$R3c$	5.638	5.638	5.638	59.35	59.35	59.35	124.73
$\text{BLEFO}_{x=0.05}$	C2	5.615	5.662	3.954	90.00	90.529	90.00	123.61
$\text{BLEFO}_{x=0.07}$	C2	7.889	5.558	2.801	90.00	90.533	90.00	122.83
$\text{BLEFO}_{x=0.1}$	C2	5.599	5.545	3.909	90.00	90.65	90.00	121.39

patterns were simulated to know the structure and lattice parameter of $\text{BLEFO}_{x=0.05,0.07,0.1}$. The crystal structure parameters derived from simulation are listed in table 1. The small R values of refinements, R_{wp} , suggest that the simulated XRD patterns agree well with the measured XRD patterns. From XRD it is confirmed that pure BFO (figure 1a) possesses single-phase rhombohedrally distorted structure $R3c$ with no trace of other (or impurity) phase within the limitation of XRD (Wang *et al* 2004; Yuan *et al* 2006). The XRD pattern indicates a structural change on doping of both La and Er. The best fit to the measured data for $\text{BLEFO}_{x=0.05}$ is observed using monoclinic type with C2 space group, indicating that with 10% of La and 5% of Er substitution the structure of BFO is transformed from rhombohedral $R3c$ to the monoclinic C2. For 10 mol% of La and 7 mol% of Er substitution, the structure is still monoclinic C2. On further increase of Er the structure remains in the same monoclinic structure (C2) indicating the ferroelectric nature of the $\text{BLEFO}_{x=0.1}$ but from structural refinement it is clear that the structure is very close to monoclinic $C2/c$ which is centrosymmetric. So $\text{BLEFO}_{x=0.1}$ exhibit pseudomonoclinic C2 symmetry. The above result is also reflected in Raman and ferroelectric properties. As described above there is a continuous change in crystal structure in $\text{BLEFO}_{x=0.05,0.07,0.1}$ indicating continuous collapse of the space-modulated spin structure, which was confirmed by continuous increase in magnetization with increasing x (described in magnetic studies).

In our compositions both La^{3+} and Er^{3+} substitute Bi^{3+} ion. Since the ionic radius of La^{3+} is greater than the ionic radius of Bi^{3+} (≈ 0.014 nm) and the ionic radius of Er^{3+} is smaller than the ionic radius of Bi^{3+} (≈ 0.014 nm), it is expected that the unit cell volume change should be minimum. Table 1 confirms this fact. But by keeping La doping percentage fixed and by increasing Er concentration, one would expect a subsequent decrease in volume since the ionic radius of Er is less than that of Bi. From the table it is clear that the volume of primitive unit cell decreases with increase in Er doping. This confirms the fact that the amphoteric Er substitute Bi site. More supporting evidence is provided in Raman spectroscopy.

3.2 DTA

Figure 2 shows the DTA curves of BFO and $\text{BLEFO}_{x=0.05,0.07,0.1}$ samples for both cooling and heating

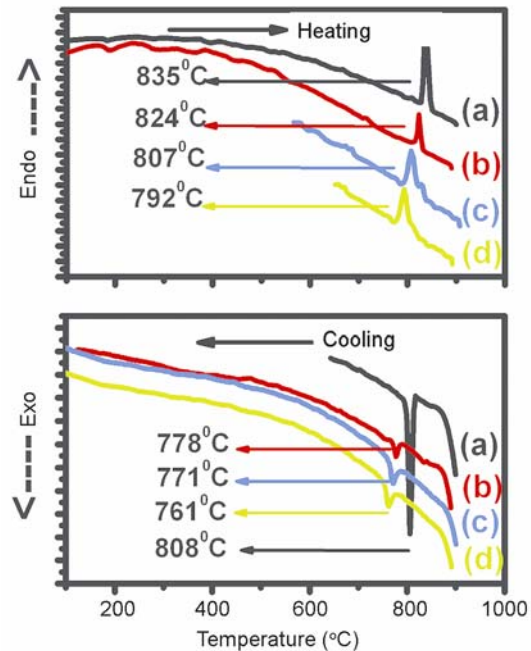


Figure 2. DTA curves for (a) BFO, (b) $\text{BLEFO}_{x=0.05}$, (c) $\text{BLEFO}_{x=0.07}$, (d) $\text{BLEFO}_{x=0.1}$ for both cooling and heating cycles.

cycles at the rate of 10°C/min. BFO undergoes a structural transition at 835°C which can be attributed to the ferroelectric ordering temperature (T_c). The endothermic peak at 835°C in the heating cycle signifies this phase transition. The same peak appears at 808°C while cooling implying a first-order phase transition. This peak corresponds to ferroelectric to paraelectric transition temperature of pure BFO. Figures 2(b–d) clearly show the decrease in T_c on subsequent Er doping for $\text{BLEFO}_{x=0.05,0.07,0.1}$. The ferroelectric transition decreased (during heating) from 835°C (BFO) to 792°C (in case of $\text{BLEFO}_{x=0.1}$). Ion modification lowered the ferroelectric phase transition temperature which may be attributed to defects generated due to doping (Kim *et al* 2002).

3.3 Raman studies

Raman scattering spectra at room temperature was deconvoluted and the obtained peaks were compared with the recent published literature data (Singh *et al* 2006; Fukumura *et al* 2007; Yuan *et al* 2007). Group theory has

Table 2. Observed and reported Raman modes for BFO and observed Raman modes for $\text{BLEFO}_{x=0.05,0.07,0.1}$.

Raman modes (cm^{-1})	Yuan <i>et al</i> 2007 (BFO)	Singh <i>et al</i> 2006 (BFO)	Fukumura <i>et al</i> 2007 (BFO)	BFO present study	$\text{BLEFO}_{x(x=0.05)}$	$\text{BLEFO}_{x(x=0.07)}$	$\text{BLEFO}_{x(x=0.1)}$
A_1^{-1}	126	136	147	126	137	137	138
A_1^{-2}	165	168	176	167	168	169	171
A_1^{-3}	213	211	227	217	236	234	233
A_1^{-4}	425	425	490	490	515	492 ^a	537
E^{-2}	259.5	275	265	259	275	283	281
E^{-3}	—	335	279	280	316	—	313
E^{-4}	339.6	365	351	327	348	—	359
E^{-5}	366.9	—	375	365	—	381	—
E^{-6}	473.3	456	437	—	414	—	479
E^{-7}	599.6	597	525	597	622	618	610
E^{-1}	111.7	77	—	—	108	108	101

^aVery broad; ^boverlap on broad 414 cm^{-1} peak.

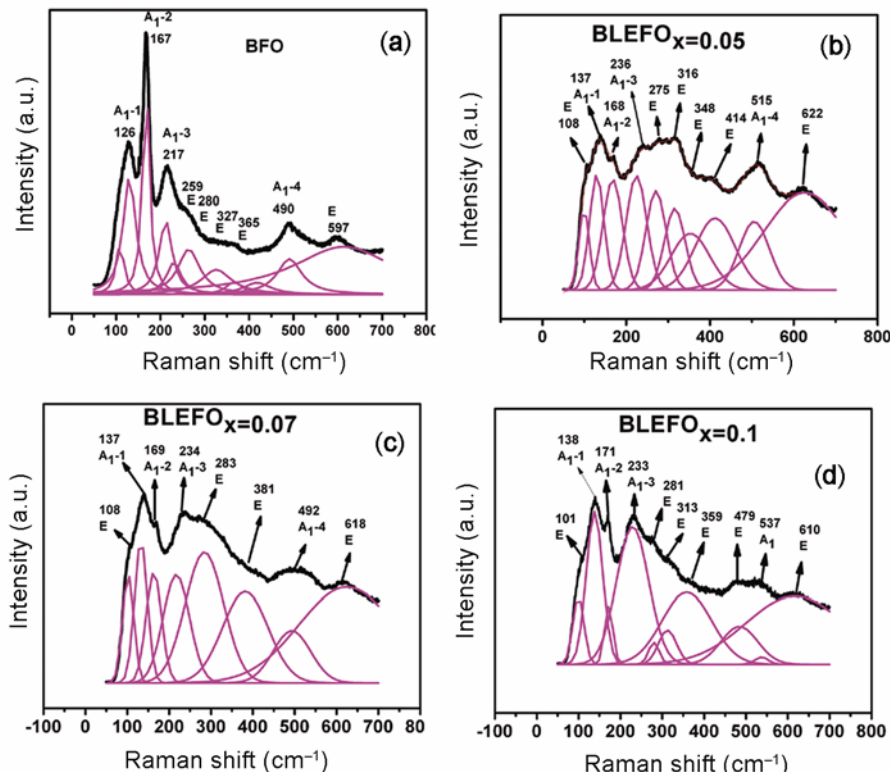


Figure 3. Measured Raman scattering spectra and deconvoluted active modes for (a) BFO, (b) $\text{BLEFO}_{x=0.05}$, (c) $\text{BLEFO}_{x=0.07}$, (d) $\text{BLEFO}_{x=0.1}$ samples at room temperature.

predicted 13 Raman active phonons represented by $\Gamma = 4A_1 + 9E$. Figure 3 shows comparison of normalized Raman spectra of BLEFO_x samples with those of the BFO samples. The reported Raman peak position of BFO is illustrated in table 2. The observed data for BFO is in close agreement with that of Yuan *et al* (2007). Raman scattering data clearly shows four intense peaks of high intensity at (126 cm^{-1} , 167 cm^{-1} , 217 cm^{-1} and 490 cm^{-1}) corresponding to the A modes (A_1^{-1} , A_1^{-2} , A_1^{-3} and A_1^{-4}),

whereas five E peaks are visible at 259 cm^{-1} , 280 cm^{-1} , 327 cm^{-1} , 365 cm^{-1} and 597 cm^{-1} . The Raman peak observed at 490 is very broad, may be due to coexistence of A_1^{-4} and E -6 modes (table 2). A shift was observed in the A modes (A_1^{-1} , A_1^{-2} , A_1^{-3} and E -2 modes) towards higher wavenumber for $\text{BLEFO}_{x=0.05}$, $\text{BLEFO}_{x=0.07}$ and $\text{BLEFO}_{x=0.1}$. With increasing Er percentage, the intensities of A_1^{-1} , A_1^{-2} , A_1^{-3} and E -1 modes decrease and the peaks are broadened. According to Yuan *et al* the stereochemical activity of Bi

ion electron pair plays the main role in the change of both Bi–O covalent bonds which reflects in five (E-1, A_1^{-1} , A_1^{-2} , A_1^{-3} and E-2) characteristic modes. These modes are responsible for the ferroelectric nature of the BFO samples. The presence of A-site ion disorder commonly brings a continuous and slow change for mode intensity. The change in Bi–O covalent bonds near FE–PE transition leads to faster drop in mode intensity. So in our case the broadening of the Raman peaks as well as the decrease in the intensity of the Raman peaks (corresponding to A_1 and E-1 modes) is attributed to the A-site substitution of Bi ions by Er which leads to a decrease in the stereochemical activity of the Er doped BFO. This further emphasizes the fact that Er has been substituted for A-site despite its amphoteric nature. The intensities of peaks of other E modes are quite low and appeared at 280, 327, 365 and 597 cm^{-1} for pure BFO. The intensities of these E modes are further decreased and indistinguishable in case of La and Er doped BFO samples.

3.4 Magnetic studies

BiFeO_3 has known to be antiferromagnetic with a G-type magnetic structure but has a residual magnetic moment due to a canted spin structure (Ruette *et al* 2004; Lee *et al* 2006). Figure 4 shows the magnetization hysteresis (M - H) loops of BFO and $\text{BLEFO}_{x=0.05,0.07,0.1}$ samples for the maximum magnetic field (H_m) of 8 Tesla. This is evident from figure 4 that pure BiFeO_3 behaves like an anti-ferromagnet, whereas increased magnetization is observed with increased Er content. Weak magnetization (M_r) of 0.076 emu/g is observed in $\text{BLEFO}_{x=0.05}$. The M_r increases as Er doping percentage increases. In case of $\text{BLEFO}_{x=0.07}$ the M_r increases to 0.1164 emu/g which further increases to 0.1178 emu/g in case of $\text{BLEFO}_{x=0.1}$.

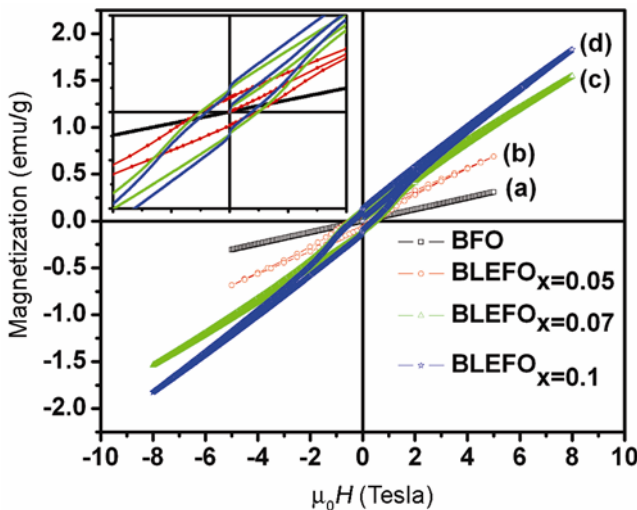


Figure 4. Magnetization hysteresis (M - H) loops of BFO, $\text{BLEFO}_{x=0.05}$, $\text{BLEFO}_{x=0.07}$ and $\text{BLEFO}_{x=0.1}$.

The appearance of ferromagnetism in the $\text{BLEFO}_{x=0.05,0.07,0.1}$ ceramics may arise due to the destruction of spin cycloid structure and result in limited increase of magnetization. Structural transformation (due to La and Er doping) destroys the spin cycloid and release the latent magnetization locked within the cycloid resulting in enhancement of magnetic properties (Cheng *et al* 2008; Pandit *et al* 2009). Here the question arises whether M_r and H_c in $\text{BLEFO}_{x=0.05,0.07,0.1}$ truly arises from the collapse of the space modulated spin structure or it is caused by other factors such as presence of Fe_2O_3 and/or impurity phases and the change from canted antiferromagnetic order to ferromagnetic order. The clarification is as follows based on the article by (Yuan *et al* 2006). The $\text{BLEFO}_{x=0.05,0.07,0.1}$ samples have larger H_c ($\approx 8\text{ kOe}$) compared to Fe_2O_3 impurity ($< 100\text{ Oe}$). Thus it is quite unlikely that this small M_r is a result of small Fe_2O_3 impurity present in the material. The Curie temperature of other impurity phases, if present, is much lower than the room temperature, which indicates the null effect of impurity on M_r . The samples exhibit small magnetization compared to nominal ferromagnetic compounds and could be termed as weakly ferromagnetic. Hence the magnetization observed in $\text{BLEFO}_{x=0.05,0.07,0.1}$ is due to collapse of spiral spin structure.

3.5 Dielectric studies

Figure 5 illustrates the dependence of dielectric constant (ϵ'_r) and loss tangent ($\tan \delta$) on frequency for BFO and $\text{BLEFO}_{x=0.05,0.07,0.1}$ at room temperature. For all composition the dielectric constant remains fairly constant in studied frequency-range (100 Hz–1 MHz). At room temperature in all frequency range, the dielectric constant of

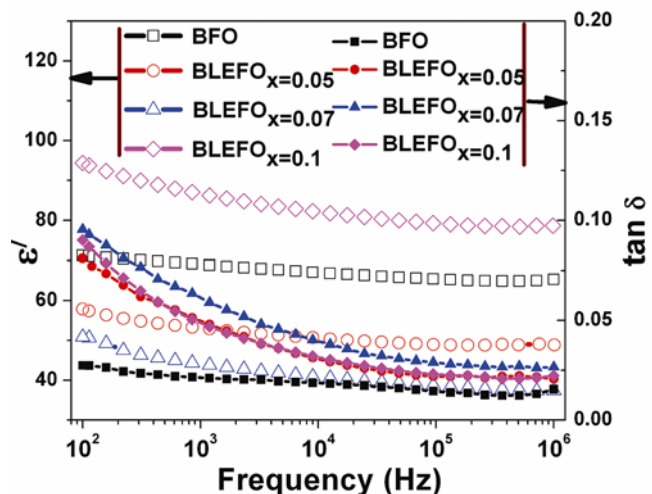


Figure 5. Variation of dielectric constant and dielectric loss tangent with frequency (100 Hz to 1 MHz) at room temperature of BFO and $\text{BLEFO}_{x=0.05,0.07,0.1}$.

BFO is greater than $\text{BLEFO}_{x=0.05}$. With further substitution of Er (7 mol%) the dielectric constant of BFO decreases further. But by further increase in Er concentration (10 mol%) the dielectric constant increases in comparison to BFO. The dielectric constant at 1 kHz of different composition at room temperature can be summarized as $\epsilon'_r(\text{BLEFO}_{x=0.1}) \approx 85 > \epsilon'_r(\text{BFO}) \approx 68 > \epsilon'_r(\text{BLEFO}_{x=0.05}) \approx 52 > \epsilon'_r(\text{BLEFO}_{x=0.07}) \approx 43$. The dissipation factor ($\tan \delta$) for BFO is almost constant (0.015) in measured frequency range. The dielectric loss increases (but remain below 0.028 at 1 MHz) for $\text{BLEFO}_{x=0.05,0.07,0.1}$ ceramics at room temperature compared to BFO. For $\text{BLEFO}_{x=0.05,0.07,0.1}$ the ($\tan \delta$) value increases slightly from 0.028 to 0.09 with decrease in frequency. This small increase in $\tan \delta$ in low frequency range corresponds to small increase in conductivity of the samples. The decrease in intrinsic dielectric constant of $\text{BLEFO}_{x=0.05}$ and $\text{BLEFO}_{x=0.07}$ compared to BFO confirms the structural changes after Er and La doping. Similarly, the increase in intrinsic dielectric constant of $\text{BLEFO}_{x=0.1}$ compared to BFO, $\text{BLEFO}_{x=0.05}$ and $\text{BLEFO}_{x=0.07}$ describes the structural changes which are somehow different from the structure of $\text{BLEFO}_{x=0.05,0.07}$. These results indicate that the dielectric behaviour of BFO and $\text{BLEFO}_{x=0.05,0.07,0.1}$ ceramics may be dependent on the crystal structure.

3.6 Ferroelectric properties

Figure 6 shows plots of polarization hysteresis ($P-E$ loops) of BFO, $\text{BLEFO}_{x=0.05,0.07,0.1}$ samples measured at 50 Hz. Well-saturated ferroelectric loops of BFO and $\text{BLEFO}_{x=0.05,0.07}$ have been obtained due to low leakage current ($\approx 17 \text{ mA/m}^2$ at 100 kV/cm). No saturated ferroelectric loop was observed in $\text{BLEFO}_{x=0.1}$ due to the shift in the paraelectric region for the corresponding composi-

tion. The maximum polarization ($2P_r$) values obtained for BFO, $\text{BLEFO}_{x=0.05}$ and $\text{BLEFO}_{x=0.07}$ are $18.4 \mu\text{C}/\text{cm}^2$ (at 160 kV/cm), $16.3 \mu\text{C}/\text{cm}^2$ (at 170 kV/cm) and $13.4 \mu\text{C}/\text{cm}^2$ (at 185 kV/cm) respectively. In case of $\text{BLEFO}_{x=0.1}$, the polarization value ($2P_r$) obtained was $1.8 \mu\text{C}/\text{cm}^2$ at an applied field of 100 kV/cm. As noted by (Yuan *et al* 2006) the mechanism of ferroelectricity is different from that of perovskites. Here a lone s^2 electron pair of A-site Bi^{3+} may hybridize with an empty p orbital, which forms a localized lobe, causing a structural distortion and introducing ferroelectricity. Since the ferroelectricity is caused due to the A-site Bi^{3+} ions, above a certain substitution of the A-site Bi^{3+} ions may lead to the transition from FE to PE region as indicated by the dielectric and ferroelectric curves of $\text{BLEFO}_{x=0.1}$.

4. Conclusions

BFO and $\text{BLEFO}_{x=0.05,0.07,0.1}$, have been successfully synthesized by conventional sintering process and their multiferroic properties have been investigated. Decrease in T_c value with subsequent Er doping indicated lowering of Curie temperature. Structural transformation of BFO was observed from rhombohedral $R3c$ to monoclinic $C2$ for simultaneous La and Er doping. It was observed that the magnetic properties of pure BFO have been improved by Er doping and weak ferromagnetism was observed with subsequent Er doping. Dielectric permittivity was constant at all frequencies and low dielectric loss was observed for all compositions. Proper ferroelectric hysteresis loop is obtained for BFO. The decrease in ferroelectric polarization was observed for Er doped samples due to the decrease in the stereochemical activity of the A-site ions. It implied that erbium doped BLEFO_x samples exhibited improved magnetic and reasonable ferroelectric properties for low levels of doping.

Acknowledgements

The authors acknowledge the help received from Mr M K Singh, Mr Prem Kumar and Dr Indranil Bhaumik for characterizations.

References

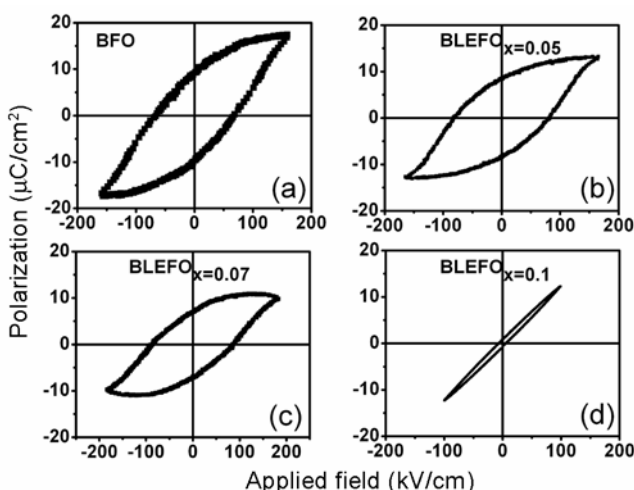


Figure 6. Polarization hysteresis ($P-E$) loops of (a) BFO, (b) $\text{BLEFO}_{x=0.05}$, (c) $\text{BLEFO}_{x=0.07}$ and $\text{BLEFO}_{x=0.1}$ samples.

- Cheng X, Li A H, Wang X L, Dou S X, Ozawa K, Kimura H, Zhang S J and Shrout T R 2008 *J. Appl. Phys.* **103** 07E507
- Cheong S W and Mostovoy M 2007 *Nat. Mater.* **6** 13
- Chung C F, Lin J -P and Wu J -M 2006 *Appl. Phys. Lett.* **88** 242909
- Dho X, Qi J, Tomov R, Blamire M G and MacManus-Driscoll J L 2006 *Appl. Phys. Lett.* **86** 062903
- Ederer C and Spaldin N A 2005 *Phys. Rev. B* **71** 060401(R)
- Eerenstein W, Morrison F D, Dho J, Blamire M G, Scott J F and Mathur N D 2005 *Science* **307** 1203a

- Eerenstein W, Mathur N D and Scott J F 2006 *Nature* **442** 759
- Fischer P, Polomskya M, Sosnowska I and Szymanksi M 1980 *J. Phys.* **C13** 1931
- Fukumura H, Harima H, Kisoda K, Tamada M, Noguchi Y and Miyayama M 2007 *J. Magn. Magn. Mater.* **310** e367
- Hill N A 2004 *J. Phys. Chem.* **B104** 6694
- Jun Y K, Moon W T, Chang C M, Kim H S, Ryu H S, Kim J W, Kim K H and Hong S H 2005 *Solid State Comm.* **135** 133
- Kim T Y, Jang H M and Cho S M 2002 *J. Appl. Phys.* **91** 336
- Kumar M M, Srinivas V R K and Suryanarayanan S V 2000 *Appl. Phys. Lett.* **76** 2764
- Lebeugle D, Colson D, Forget A, Viret M, Bataille A M and Gukasov A 2008 *Phys. Rev. Lett.* **100** 227602
- Lee S, Ratcliff W, Cheong S W and Kiryukhin V 2008 *Appl. Phys. Lett.* **92** 192906
- Lee Y H, Wu J M and Lai C H 2006 *Appl. Phys. Lett.* **88** 042903
- Neaton J B, Ederer C, Waghmare U V, Spaldin N A and Rabe K M 2005 *Phys. Rev.* **B71** 014113
- Pandit P, Satapathy S, Gupta P K and Sathe V G 2009 *J. Appl. Phys.* **106** 114105
- Qi X, Dho J, Tomov R, Blamire M G and MacManus-Driscoll J L 2005 *Appl. Phys. Lett.* **86** 062903
- Ruette B, Zvyagin S, Pyatakov A P, Bush A, Li J F, Belotelov V I, Zvezdin A K and Viehland D 2004 *Phys. Rev.* **B69** 064114
- Singh M K, Jang H M, Ryu S and Jo M H 2006 *Appl. Phys. Lett.* **88** 042907
- Singh S K, Ishiwara H and Maruyama K 2006 *Appl. Phys. Lett.* **88** 262908
- Sosnowska I, Lowenhaupt M, David W I F and Ibberson R M 1992 *Physica* **B180** 117
- Wang Y P, Zhou L, Zhang M F, Chen X Y, Liu J -M and Liu Z G 2004 *Appl. Phys. Lett.* **84** 1731
- Yuan G L and Or S W 2006 *J. Appl. Phys.* **100** 024109
- Yuan G L, Or S W, Liu J M and Liu Z G 2006 *Appl. Phys. Lett.* **89** 052905
- Yuan G L, Or S W and Chan H L W 2007 *J. Appl. Phys.* **101** 064101
- Zhang S T, Lu M H, Wu D, Chen Y F and Ming N B 2005 *Appl. Phys. Lett.* **87** 262907
- Zhang S T, Zhang Y, Lu M H, Du C L, Chen Y F, Liu Z G, Zhu Y Y and Ming N B 2006 *Appl. Phys. Lett.* **88** 162901
- Zhang Y, Yu S and Cheng J 2010 *J. Euro. Ceramic Soc.* **30** 271